

RESEARCH LETTER

Open Access



Deformation characteristics and instability mechanism of large-scale anti-dip rock slides

Xuebing Wang^{1,2}, Nan Zhang^{1*}, Zhihua Zhang^{3*}, Luqi Wang⁴, Shu Yu², Peng Zhao² and Guoqiang Yan⁵

Abstract

The anti-dip bedding rock slopes have threatened global infrastructure construction and urban expansion seriously. Taking the Guang'an Village rockslide as an example, this paper firstly studied the deformation characteristics of the rockslide with anti-dip bedding structure based on in-situ investigation and monitoring, and then the relevant influencing factors were summarized. On this basis, a new evolution model of continuous-pushing-section pressing locked-section and the instability mechanism of the rock slope were proposed. Finally, the applicability of the model and the deformation tendency of the rock slope were further discussed. A catastrophic sliding event has once occurred in the Guang'an Village rockslide in 2017, after which the deformation of the potential source area III (PSA-III) was accelerating. The presence of the sliding-prone geological structure provides the basic conditions for the deformation of the rock slope and the development of the sliding zone. Rainfall is the major external trigger that promotes the deformation. As the sliding zone extends forward, the overlying deformation body will keep on pushing against the preceding rock mass, which will contribute to the forward extension of the sliding zone as well. When the final locked section is crushed, the rock slope will lose balance. According to the observation in the field, the PSA-III is in the late stage of the deformation-increasing phase currently. This study can provide a reference for the analysis of failure mechanism and the design of monitoring and mitigation of other large anti-dip bedding rock slides.

Keywords Anti-dip rockslide, Instability mechanism, Deformation characteristic, Geostucture prone to sliding, Rainfall-induced rockslide

Introduction

Anti-dip bedding rock slides generally refer to rock landslides that occur on slopes where the inclination of the rock formation is opposite to that of the slope while the trend is roughly the same (Goodman and Bray

1976; Cruden 1989; Yin et al. 2023). This concept is also referred to as “anaclinal rock slope” or “counter-tilted rock slope” in some research. In this paper, “rock slopes” refers to those slopes that may not exhibit obvious signs of deformation but possess distinct sliding-prone structures, as well as rock slopes that exhibit certain degrees of deformation. In the early years, there was not much attention on the counter-tilted rock slopes as they were considered to be more stable compared with dip slopes. The anaclinal slopes came into view gradually with the rapid development of urbanization and the construction of infrastructure projects in areas with complex geological conditions (de Freitas and Watters 1973). The Afton open-pit mine in Canada, the Shiziping and Jinping hydropower station in China, and numerous highways traveling through mountain areas all over the world have

*Correspondence:

Nan Zhang
geozhangn@126.com
Zhihua Zhang
zzh_killer@126.com

¹ China Institute of Geo-Environment Monitoring, Beijing, China

² Chongqing 208 Geological Environment Research Institute Co. Ltd, Chongqing, China

³ 208 Geological Team, Chongqing Geological and Mineral Exploration Bureau, Chongqing, China

⁴ School of Civil Engineering, Chongqing University, Chongqing, China

⁵ China Three Gorges Group Corporation, Wuhan, China



© The Author(s) 2024. **Open Access** This article is licensed under a Creative Commons Attribution 4.0 International License, which permits use, sharing, adaptation, distribution and reproduction in any medium or format, as long as you give appropriate credit to the original author(s) and the source, provide a link to the Creative Commons licence, and indicate if changes were made. The images or other third party material in this article are included in the article's Creative Commons licence, unless indicated otherwise in a credit line to the material. If material is not included in the article's Creative Commons licence and your intended use is not permitted by statutory regulation or exceeds the permitted use, you will need to obtain permission directly from the copyright holder. To view a copy of this licence, visit <http://creativecommons.org/licenses/by/4.0/>.

suffered from this kind of rock slope hazards (Reid and Stewart 1986; Sagaseta et al. 2001; Qi et al. 2004; Liu et al. 2016; Zhou et al. 2023).

In fact, the anti-dip landslides are widespread in folded mountains, and plenty of research has been carried out on the failure mechanism of this kind of geohazard (Huang and Li 2011; Yin et al. 2016). Besides being counter-tilted, the rock layers often have a slip-prone structure of alternate hard and soft layers. Meanwhile, a mass of joints and fissures perpendicular to the rock faces is often developed in the deforming rock mass (Cruden and Krahn 1973). Those characteristics of this geotstructure prone to sliding were primarily developed under tectonic actions, gravitational forces, lithological properties, weathering, and various human engineering disturbances (Huang et al. 2012).

The methods adopted in the study of failure mechanisms include analytical methods, numerical simulations, and physical experiments (Zhang et al. 2022d, 2024; Gao et al. 2023; Yin et al. 2024). Goodman and Bray (1976) firstly proposed an analytical method for toppling which has been widely used due to its simplicity. The cantilever beam model is also an effective way to analyze the stability of antidip slopes (Bucek 1995). For intricate ones, numerical simulation is an appropriate technique. Gu and Huang (2016) have presented the complex deformation and failure characteristics of Gongjiangfang rockslide through UDEC. Cui et al. (2022) evaluated the impact of underground coal mining on Pusa landside by the discrete element model as well. As to physical experiments, centrifuge simulation is of advantages in studying the failure mode by generating centrifugal force (Zhang et al. 2022a, b, 2023a). Adhikary et al. (1997) investigated the toppling mechanism of slope models of both brittle and plastic materials by means of centrifugal model tests. Huang et al. (2022) studied the deformation and failure mechanism of the reverse inclined slope with the soft-hard interlayer structure by centrifuge as well.

The research above has all achieved good results and enriched the understanding of anti-dip rock slides. However, most of them focused more on the mechanical modeling and analysis of the structure of the bedding slopes, and less attention has been paid to the internal and external geodynamic effects in the growth environments of the rock mass. In the natural world, the deformation process and failure mechanisms of landslides are extremely complex. The internal geodynamic effects have a direct impact on the formation and composition of landslides, whereas the external geodynamic effects directly influence the deformation process (Wang et al. 2023; Yin et al. 2023). These processes play a crucial role in the exploration of the deformation process and instability mechanisms in anti-dip rock slopes. However, these

processes are filled with various uncertainties, making it difficult to replicate them through numerical simulation or physical modeling.

Therefore, to investigate the deformation process and instability mechanisms of a real landslide under the coupled effects of internal and external forces, it is beneficial to employ indirect analytical methods (Dai et al. 2021). Firstly, a comprehensive assessment of its primary geological structures and deformation features should be conducted. Subsequently, an in-situ monitoring approach can be utilized to gather relevant data. Through further analysis of these in-situ monitoring data, it becomes feasible to effectively reconstruct the deformation process of the landslide. For example, Zhang et al. (2021) have found a correlation between daily deformation and hydrological inducing factors by analyzing long-term in-situ monitoring data of the Taping landslide.

This, in turn, allows for the deformation modes and instability mechanisms that are more representative of the real situation. However, at present, there is a limited amount of research evaluating the influence of external forces on the deformation of anti-dip rockslides using in-situ monitoring methods. Besides, there is a necessity for proper models of instability analysis based on deformation characteristics in practical surveys, monitoring, and early warning projects of counter-tilt rock slides. However, currently, there is limited research that has proposed the failure mechanisms or established evolution modes from the perspective of field monitoring of rock slides.

In this paper, an evolution model and instability mechanism for the anti-dip rock slope have been proposed on the basis of deformation characteristics of a typical anti-dip bedding rockslide-Guang'an Village rockslide in Wuxi, Chongqing, China. After an introduction of the geological background of the rockslide, the deformation features of the slipped area and the potential source area III (PSA-III) were presented according to field investigation and monitoring. The slipped area and the PSA-III stand out as the areas within the Guang'an Village rockslide that exhibit the most intense deformation, making them the primary focus of this research. Then, the influencing factors that caused deformation were summarized. The evolutionary mode of continuous-pushing-section pressing locked-section was proposed along with its failure mechanism. Finally, the relationship between rainfall and deformation was studied quantitatively by Pearson correlation coefficient (PCC) analysis in PSA-III. The applicability of the instability model and the deforming trend of PSA-III were discussed, respectively. The relevant monitoring method was suggested. This work could provide a reference for research with regard to the deformation and failure mechanism analysis and

monitoring and early warning of similar rock slides with anti-dip bedding structure.

Materials

In this section, we would start by providing an overview of the general geological and environmental conditions of the Guang’an Village rockslide, as well as its spatial zoning. It must be noted that, the overall geological and environmental background, as well as spatial zoning of the Guang’an Village rockslide are not the primary focus of this study.

The geological and zoning data are mainly derived from geological investigations conducted in 2017, carried out promptly after the significant sliding event in Guang’an Village. Wang et al. (2019) has reported the sliding event and analyzed the geological model of the Guang’an Village rockslide in detail. After that, Zhang et al. (2022c) analyzed the spatial–temporal evolution of post-event deformation of the slipped area after the landslide event based on the time-series results. Qin et al. (2022) reproduced the landslide event and predict the potential accumulation characteristics that could be brought about by the failure of the PSA-III by a granular flow model and an elasto-visco-plasticity model. Zhang et al. (2023b)

studied the dynamic process of the Guang’an Village landslide of the slipped area.

Based on those background, we would then proceed to examine the material composition and structural characteristics of the slipped area and the PSA-III.

Geological and environmental conditions

The Guang’an Village rockslide is located in Wuxi County, Chongqing, China, with the central coordinates of E 109°36′57″ and N 31°32′15″, as shown in Fig. 1. Seating on the left bank of the Xixi River, the whole slope orientation of the rock hill is 181° with an elevation between 280 and 1130 m.a.s.l. The highest point in the area is on the top of the hillside with an altitude of up to 1410 m.a.s.l., while the lowest position was found on the riverbed of the Xixi River at about 276 m.a.s.l. The overall terrain of the landslide is steep in the upper part (40°–50°) and gentle in the lower part (25°–35°).

As to the regional tectonics, the landslide area is situated within the Dabashan fold belt where a series of east–west anticlines and synclines are seated in parallel. The source area of the rockslide lies on the northward-dipping limb of a subsidiary anticline belonging to Bangbangliang-Maoerbei synclinorium, whose trend of axis travels from 100° to 120°. The rock mass in the rock slide

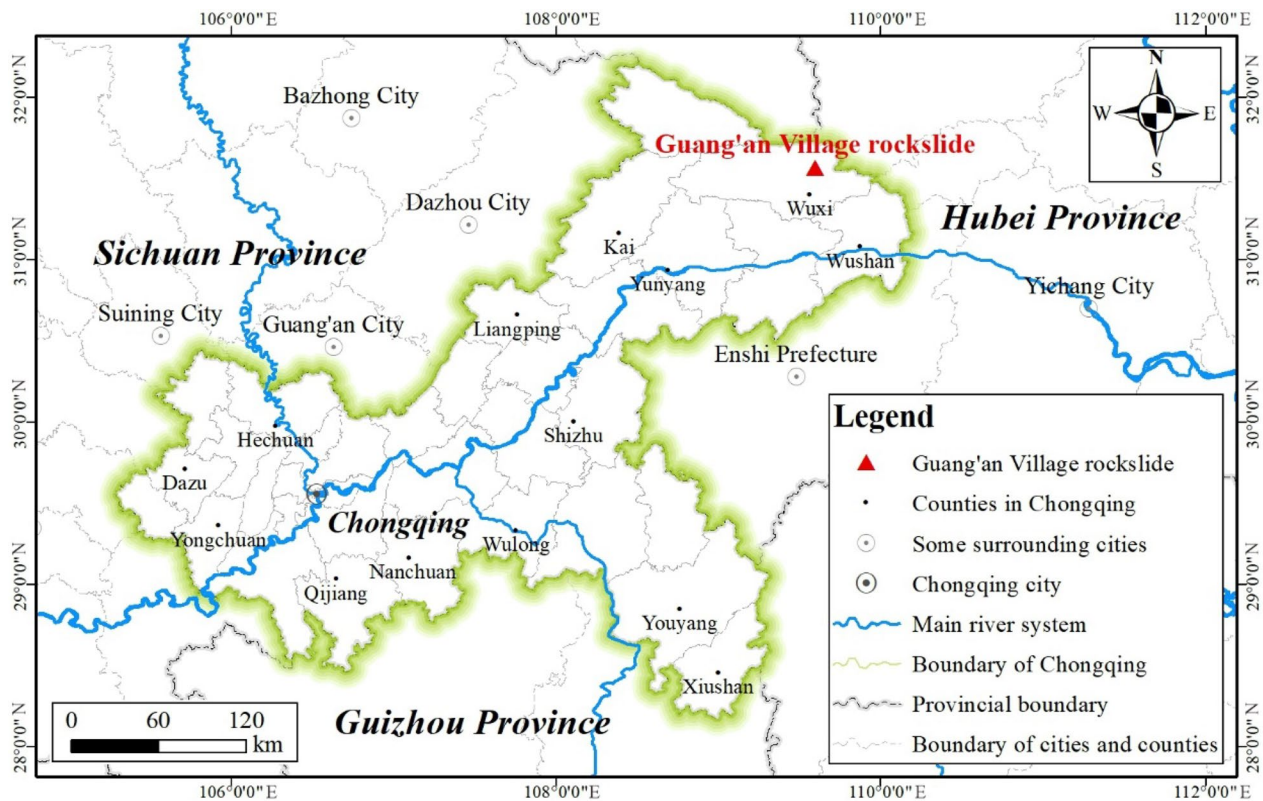


Fig. 1 Geographical location of Guang’an Village rockslide

area shows a reverse inclined structure, dipping north with an inclination angle between 28° and 46°. Many tectonic cracks and vertical joints are exposed, extending parallel to the strike of the subsidiary anticline.

The strata in the landslide area mainly include the Quaternary, Triassic, Permian, and Silurian from top to bottom. The lithology of the exposed bedrock is limestone and shale majorly. The limestone is medium thick-thick layered with coals distributed in the middle and upper part. The shale is mainly thin layered.

The annual temperature remains at 14.7 °C, and the annual rainfall reaches 1333 mm on average (Wang et al. 2019). Many gullies develop on the slope with a small amount of seasonal flowing water. Many house-building, road construction, and agricultural activities used to take place around the sliding area. In addition, coal mining activities had been carried out along the coal seams before the 1950s, which aggravated the damage to the rock slope directly to a certain extent.

Spatial zoning of Guang’an Village rockslide

The scale of the Guang’an Village rockslide is substantial. Field investigations have revealed that the landslide spans a length of 1500 m and a width of 1300 m. The estimated total volume of the landslide measures $33.5 \times 10^6 \text{ m}^3$. It has been divided into three distinct regions: the slipped area, the potential source area

(PSA), and the potential transportation area (PTA), as illustrated in Fig. 2. This zoning was determined based on field investigations and geological disaster emergency monitoring, and the detailed zoning criteria could be found in relevant references (Wang et al. 2019). Before delving into a detailed examination of the deformation characteristics of the slipped area and the PSA-III, a concise introduction is provided for each zone within the Guang’an Village rockslide.

The slipped area is the region where the 2017 large-scale sliding occurred and was further split into three parts: the source area, the transportation area, and the deposition zone. The catastrophic event that happened in 2017 will be detailed in the later section. The PSA was chopped into four regions, PSA-I, PSA-II, PSA-III and PSA-IV. The PTA was zoned as PTA-I and PTA-II. The scales of all zones are listed in Table 1, and the spatial characteristics are described separately as follows.

(1) Slipped area

Located in the middle part of the landslide area, the slipped area has the main scarp as the rear boundary with a height of about 30 m, which was formed after the violent movement in 2017, while its front edge is bounded by the Xixi River.

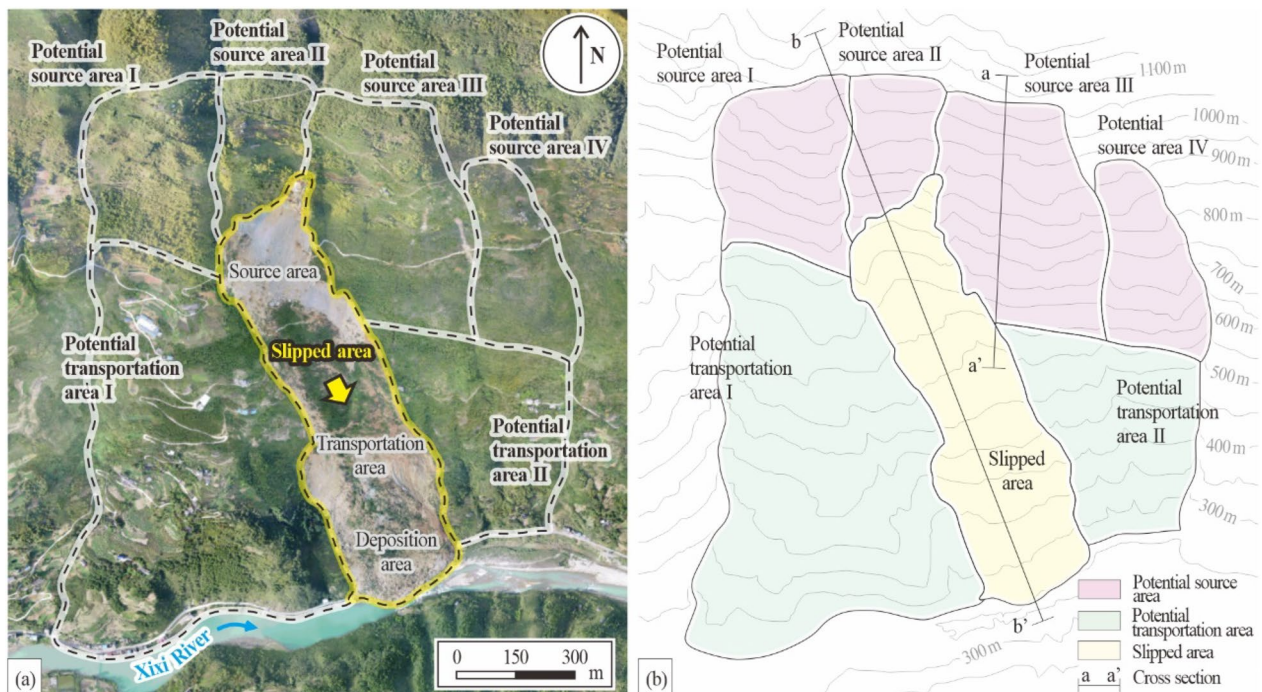


Fig. 2 a Overview and b spatial zoning of Guang’an Village rockslide

Table 1 Spatial characteristics of Guang'an Village rockslide

Major zone	Subzone	Length (m)	Width (m)	Average thickness (m)	Height difference (m)	Volume (10 ⁶ m ³)	Dip angle (°)
Slipped area	–	1200	300	25	640	8.3	50–80
PSA	I	500	300	40	360	6.0	40–50
	II	400	200	40	300	3.2	70
	III	550	450	45	200	11	50–65
	IV	450	250	45	310	5.0	45
PTA	I	800	400–800	–	450	–	20–30
	II	600	300–600	–	370	–	20–30

(2) PSA

The back edge of PSA is a continuous fracture developing at the steep-gentle junction of terrain, behind which is a steep rock slope. The leading edge is bounded by the steep-slow transition area.

The west side of the PSA is a deep gully with a V-shape whose width varies from 30 to 80 m and has a depth of about 20 m and a slope of around 45° at the bottom. The east side is a natural gully, with a cutting depth ranging from 10 to 30 m, a horizontal width between 10 and 50 m, and a longitudinal length of approximately 640 m. It spreads directly to the Xixi River.

The boundaries between each subzone are all distinct. A V-shaped seasonal gully develops between PSA-I and PSA-II, with a width of 30–60 m and a depth of about 20 m. The PSA-III has been separated from PSA-II by a U-shaped valley with a depth of about 15 m and a width of 60–80 m. The boundary between PSA-III and PSA-IV

is a ditch, extending from the back of the slide area to the Xixi River, with a depth from 5 to 30 m and a width varying from 10 to 50 m. The topographic slope of the ditch bottom varies in line with the slope surface.

(3) PTA

The PTA presents an entire slope smaller than that of the PSA. Some people reside in PTA-I, and a large area of farmland has been reclaimed in PTA-II.

Material composition and structure characteristics

In this section, the material composition and structural characteristics of the slipped area and the PSA-III would be introduced.

The material composition and structural characteristics of the Guang'an Village rockslide were revealed by field investigation and geological drilling. Typical geological profiles of the rockslide are shown in Fig. 3, where Fig. 3a

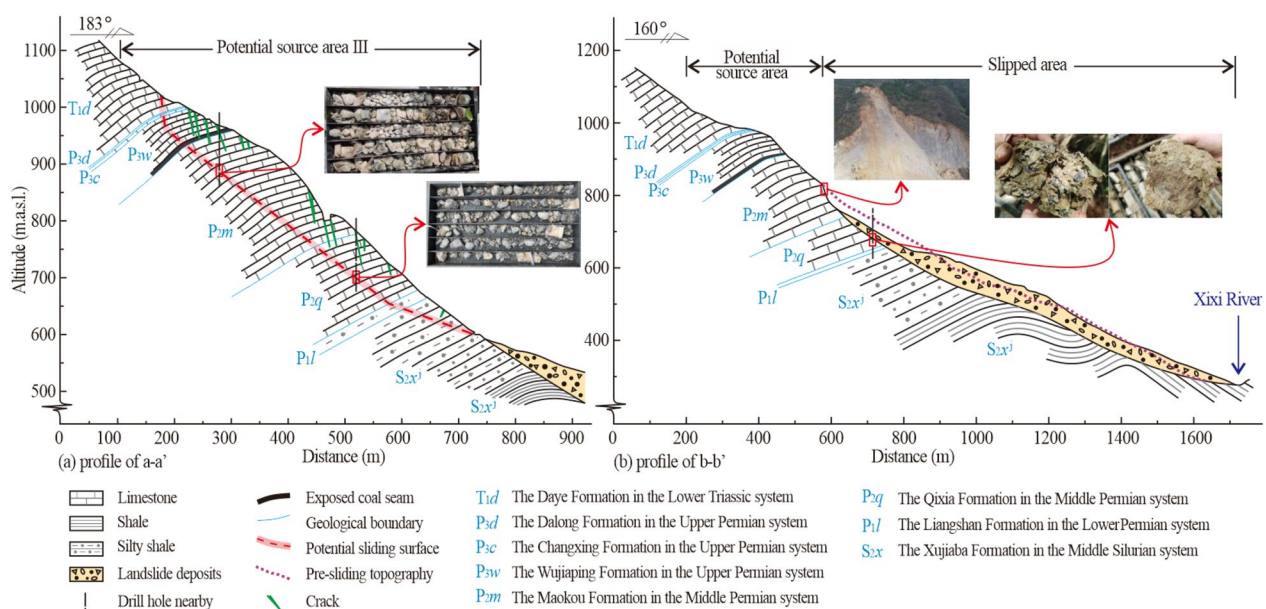


Fig. 3 Typical geological profiles of **a** PSA-III and **b** the slipped area

exhibits the structure of PSA-III, and Fig. 3b presents the section of the slipped area. The location of the profile line is marked in Fig. 2. The reason the PSA-III was chosen for the analysis in this research lies in the most obvious signs of deformation it presents, which was reported in detail by Wang et al. (2019) and Qin et al. (2022). The structure feature of PTA was not involved as the rock slope of PTA does not deform significantly.

The average thickness of the deformation body in PSA-III is 40 m–50 m. According to the drilling core, the rock between 0 and 45 m and below 50 m was of good integrity, while between 45 and 50 m, the core was broken with obvious corrosion signs as shown in Fig. 3a. This indicates that the sliding surface was located between 45 and 50 m underground.

As can be seen from Fig. 3a, the rock materials consist of limestone of Daye Formation in the Lower Triassic system (T1d), Dalong Formation, Changxing Formation, and Wujiaping Formation in the Upper Permian system (P3d, P3c, P3w), Maokou Formation and Qixia Formation in the Middle Permian system (P2m, P2q), and shale of Liangshan Formation in the Lower Permian system (P1l) and Xujiaba Formation in the Middle Silurian system (S2xj). The limestone of P3d, P3c, and P3w has a thin-medium thick bedding structure, with vast quantities of joints and fissures on the broken surface. The rock mass has long been eroded by groundwater strongly, so there are dissolved pores and gaps everywhere. Meanwhile, thin coal seams are sandwiched in the limestone locally. The limestone of P2m and P2q is thick-bedding, where the dissolution is serious as well. The thin-bedding and carbonaceous shale is distributed below the limestone.

The thickness of the source area in the slipped zone is about 25 m. As shown in Fig. 3b, a steep rock slope with an inclination of 60–80° was formed in the source area, which is exactly the rupture surface of the landslide disaster in 2017. The bedrock is composed of limestone of the Maokou Formation and Qixia Formation of the Middle Permian system (P2m, P2q), and has a massive structure with block diameters of 0.5–10 m. The rock mass is pock-marked with dissolution pores and cracks. The diameter of the solution pore is 5–20 cm. The width of fractures concentrates in 5–20 cm, and the extension length varies from 5 to 120 cm. A small amount of clay and fragmented limestone is filled in dissolving holes and fissures.

The bedrock in the transportation area and the deposition area is composed of shale of the Liangshan Formation in the Lower Permian system (P1l) and silty shale of the Xujiaba Formation in the Middle Silurian system (S2xj).

The main sliding body has parked itself in the transportation area. Although the rock mass in the middle part bulges convexly due to the internal pushing in the rock

body, its integrity is good. Even the road on it has maintained a continuous overall appearance, as can be seen clearly from Fig. 2a. In addition, through drilling and coring, it was revealed that the sliding plane is mainly composed of siltstones with a particle size of 0.5–3 cm, and strong rubbing traces are visible as shown in Fig. 3b.

The components of accumulation in the deposition area are mainly broken limestone decomposed from the sliding body and the weathered rock and soil mass on the surface of the migration area. The appearance of the deposit is loose, and the maximum diameter of the blocks reaches 10 m.

Methods

The deformation characteristics of the slipped area and the PSA-III of the Guang'an Village rockslide were primarily determined through onsite investigations and field in-situ monitoring. In addition, the Small Baseline Subset Interferometric Synthetic Aperture Radar (SBAS-InSAR) method was applied to the ascending Sentinel-1A datasets spanning from May. 2019 to Feb. 2020 in this case.

As to the slipped area, the characteristics of the large-scale sliding process are primarily determined through field investigations due to the lack of professional monitoring systems at the time the disaster occurred.

In contrast, the deformation of the PSA-III is relatively slow. Therefore, its deformation characteristics are determined through a combination of field investigations and the installation of professional monitoring systems.

Geological surveys are conducted to gather information on the boundary conditions of the PSA-III and to analyze the extensive crack features observed on the surface.

The in-situ system has been established since 2018, including displacement monitoring and fissure monitoring stations on the surface, and the inclinometers in the borehole. The data provided by the GNSS measurement stations have an accuracy of ± 2.5 mm + 0.5 ppm in area measurements and ± 5.0 mm + 0.5 ppm in height measurements. Three automatic monitoring instruments for surface cracks were adopted with an accuracy of 0.043 mm. In addition, an automated rainfall station was employed with an accuracy of 1%. All data were automatically collected in real time.

Deformation characteristics

The sliding event in the slipped area

At 0:20 a.m. on Oct. 21, 2017, a large-scale slide occurred in the slipped zone of the Guang'an Village rockslide, and approximately 8.3×10^6 m³ of rock and soil mass was released from the source area. The photos before and after the sliding are shown in Fig. 4. The major sliding body stopped after a movement of about

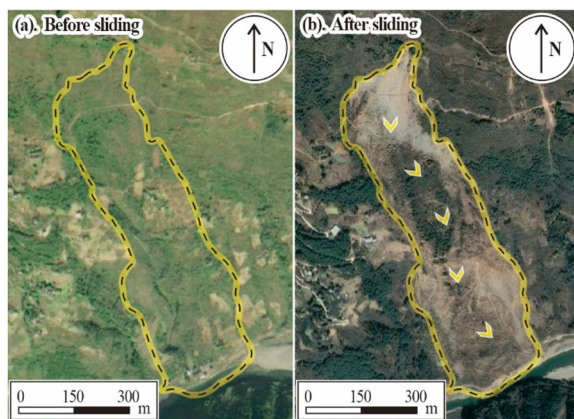


Fig. 4 Scenes of Guang'an Village rockslide **a** before and **b** after the 2017 sliding

300 m, while the other part of the rock mass continued running downhill, transferring into a debris avalanche, and forming a landslide dam on the Xixi River. The dam finally burst after a long period of scouring of river water. Some deformation features during the 2017 disaster event are described in Table 2, which were obtained through on-site investigations and interviews conducted at the homes of the villagers.

Characteristics of deformation in PSA-III

Following the large-scale landslide event in 2017, progressive deformations and surface changes have been observed in the PSA-III. Field investigation, in situ monitoring, and the interpretation of SBAS-InSAR (Fig. 5) reveal that severe deformation has been developed in the PSA-III.

If the failure of PSA-III occurs in the future, the Xixi River would be blocked again, and the safety of villages and residents downstream would be threatened once more (Zhang et al. 2022c).

Deformation on the surface

The deformation characteristics of the PSA-III were measured through on-site investigation and monitoring. The in-situ system has been established since 2018, including displacement monitoring and surface fissure monitoring stations, as shown in Fig. 6.

(1) Field investigation

The deformation signs of PSA-III were explored by site investigation, including tracing tension cracks and local collapses at the trailing edge, bulges at the middle and front part, and shear fractures at the side edges of the deforming body.

There are obvious tension cracks spreading in the back of PSA-III as shown in Fig. 7a, about 550 m long and 0.5–2 m wide. The middle and rear part of the deformable body has multiple tension fractures with local collapse as well, generally 30–70 cm wide as presented in Fig. 7c. Several bulging cracks developed on the side of Road-2 in the front part, and collapse was recorded locally as well, as shown in Fig. 7b and d. The width of the fissures is within 20 cm–80 cm, and the visible depth of the collapse reaches about 3–4 m. Figure 7e exhibits the seasonal gully with a depth varying from 5 to 30 m on the eastern border. Figure 7f presents the lateral margin fracture of the deforming mass, which is under the control of shearing, and has an overall trace of 330 m.

(2) Monitoring of ground fissures

Figure 8 shows the cumulative deformation of the three observation points of surface cracks. The monitoring period for Dg-1 and Dg-3 was from Aug. 27, 2018, to Nov. 30, 2021, and for Dg-2 was from Dec. 8, 2017, to Nov. 30, 2021. The sharp increases in the curves on Jun. 17, 2020, were induced by equipment maintenance. The Dg-1 observed a side crack at the rear edge of the

Table 2 Features of deformation during the sliding process in 2017

Time	Stage	Features of deformation
10:00 a.m Oct. 20, 2017	Before sliding	Cracks appeared in the houses and ground in the source area, about 5 m–10 m long and 1 cm–3 cm wide
3:30 p.m Oct. 20, 2017	Before sliding	The cracks were continuously expanding, up to a scale of 10 m–30 m long. A settlement of 5 cm–20 cm occurred on the surface
00:20 a.m Oct. 21, 2017	Sliding	The massive rockslide started to move from the source area, and severe deformation was formed on both sides of the slipped zone
Oct. 22–27, 2017	After sliding	Local collapses and rockslides happened frequently in the sliding area
9:00 p.m Oct. 27, 2017	After sliding	A large rock of 10,000 m ³ fell from the crown area close to PSA-III
Oct. 28, 2017	After sliding	Serious deformation occurred at the middle, rear and east side of the PSA-III with a mass of transverse and longitudinal cracks appeared

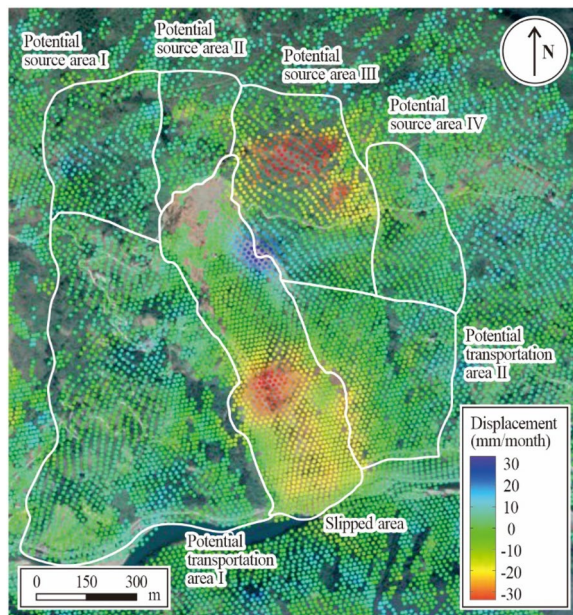


Fig. 5 Interpretation of SBAS-InSAR in Guang'an Village rockslide region from May, 2019 to Feb. 2020

main fracture belt, with a cumulative displacement of 1155 mm. The Dg-2 monitored a fissure in the main fracture belt and had recorded the largest offset of 5146 mm. The Dg-3 focused on a lateral margin fracture with a tension of 1393 mm.

Besides, while there is a period each year characterized by relatively intense and concentrated rainfall, the cumulative displacement associated with each of these periods does not demonstrate a stepwise increasing pattern. In fact, despite each concentrated rainfall period leading to intensified deformation for a certain subsequent period, the incremental displacement is decreasing year by year. This phenomenon is more pronounced in the Dg-2 curve.

(3) Displacement monitoring by GNSS

The horizontal movements of the GNSS stations from Aug. 1, 2018, to Apr. 30, 2022, are shown in Fig. 6 after being magnified by 200 times. The displacement of G-1 was only 185 mm. Its motion trail appeared to be deflected in three stages instead of generally in one direction, which might owe to the offset motion shown in Fig. 6. The accumulated horizontal moving of G-2 arrived at 829 mm with a direction slightly offset towards the slipped area. The cumulative displacement of G-3 was relatively small (271 mm).

Figure 9 demonstrates the trends of horizontal and vertical displacement of GNSS monitoring points over time.

The vertical movement of G-1 was greater than the horizontal movement, while for G-2 and G-3, the opposite pattern was presented.

These signs demonstrate that the whole moving trend of the PSA-III was downhill and deflecting toward the slipped zone. The deformation in the rear and middle region of the deforming body was large, while the displacement in the front was relatively small. This might be because the internal structure of the rock layers is more seriously damaged in the middle and rear parts of the deformable body, and there is more space available for compression and deformation. In contrast, the integrity of the internal rock in the front area is better with fewer voids, and there is less rockslide thrust transmitted from the rear side.

Underground deformation features

The subsurface deformation characteristics of the PSA-III were studied through downhole inclinometer data. The corresponding locations of two boreholes shown in Fig. 3a are illustrated in Fig. 6, labeled as Dh-1 and Dh-2, respectively. In this research, the Dh-1 borehole was chosen for subsurface displacements observing by inclinometers (labeled as In-1).

The downhole displacements were obtained by sequentially installing 67 inclinometers with an interval of 1 m in Dh-1. The underground deformation between Sep. 24, 2019, and Jan. 28, 2020, is presented in Fig. 10. Since curves had an obvious dislocation between the depth of 45 m and 50 m, that zone was considered to be where the sliding surface was located. At the same time, the movement trends of the inclinometers above the abrupt zone were very consistent, revealing that the rock mass deformed as a whole above the slip zone.

Instability mechanism

Influencing factors

Before large-scale failures in Guang'an Village rockslide, the slope body would go through a certain scale of deformation, which was mainly controlled by the topography, geological structure, lithology, goaf of coal mine, and precipitation.

(1) Topography

The overall terrain of the hillside is steep at the top while gentle at the bottom. The slope of the source area is 40–50° on the whole, where the maximum inclination exceeds 70° locally. The steep topography provided underlying conditions for the deforming in the slope body.

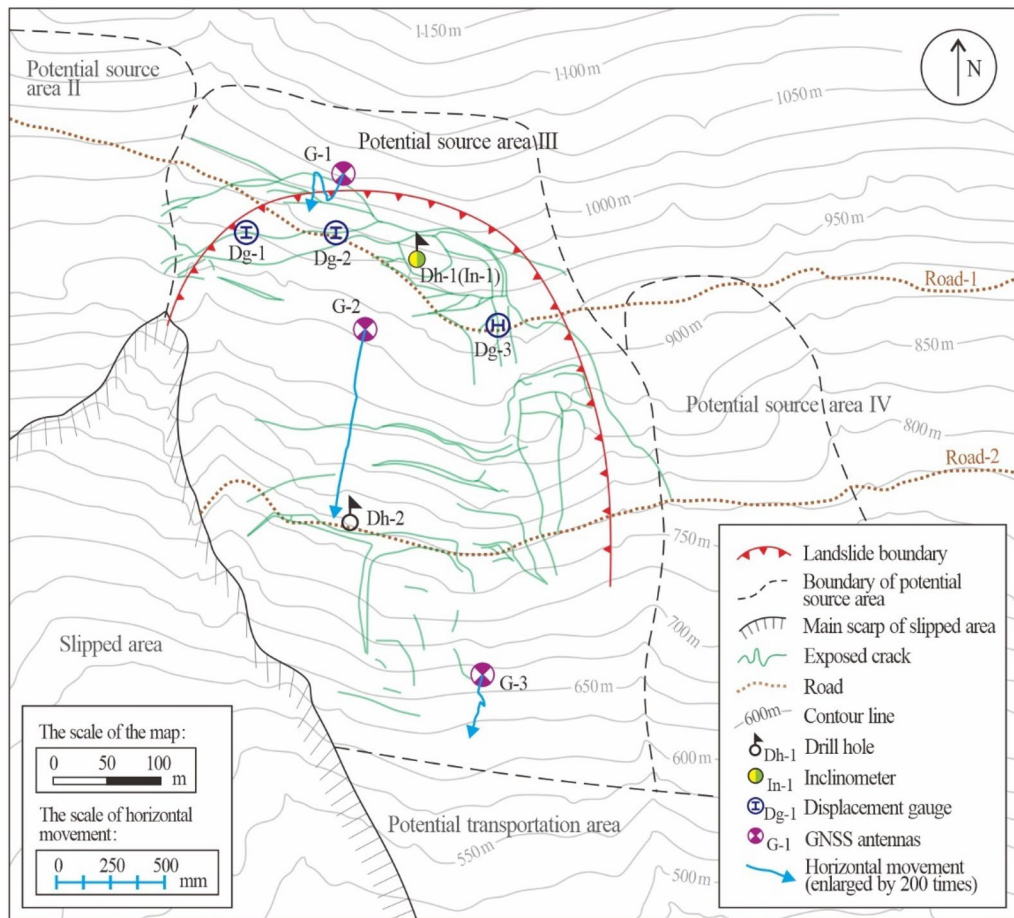


Fig. 6 Layout of in situ monitoring system in PSA-III

(2) Geological structure

The rock slope is located in the Dabashan fold belt which is currently characterized by low tectonic activity (Li et al. 2007). Under the regional tectonic stress field, multitudes of rock strata in the source area are bent, which would break the layers into serial rock blocks, and is extremely unfavorable to the stability of the slope.

(3) Lithology

The lithology in the source area of the rockslide is mainly limestone with coal seam interlayer. The soft and hard interbedding structure promotes the fracturing of the rock body.

(4) Goaf of coal mine

In the 1950s, there was coal mining in the coal layers, which further damaged the weak coal strata in the landslide area. The mined-out zones made the geological structure of the slope more susceptible to breakdown.

(5) Precipitation

The area receives an abundant annual rainfall of 1333 mm on average. The rainwater could flow into the rock mass along surface cracks, eroding limestone and carrying away some solid particles in fracture zones, stimulating the formation of karst caves and cracks inside the rock body (Ng et al. 2022). These dissolution processes mainly occur along the bedding planes and existing fractures.

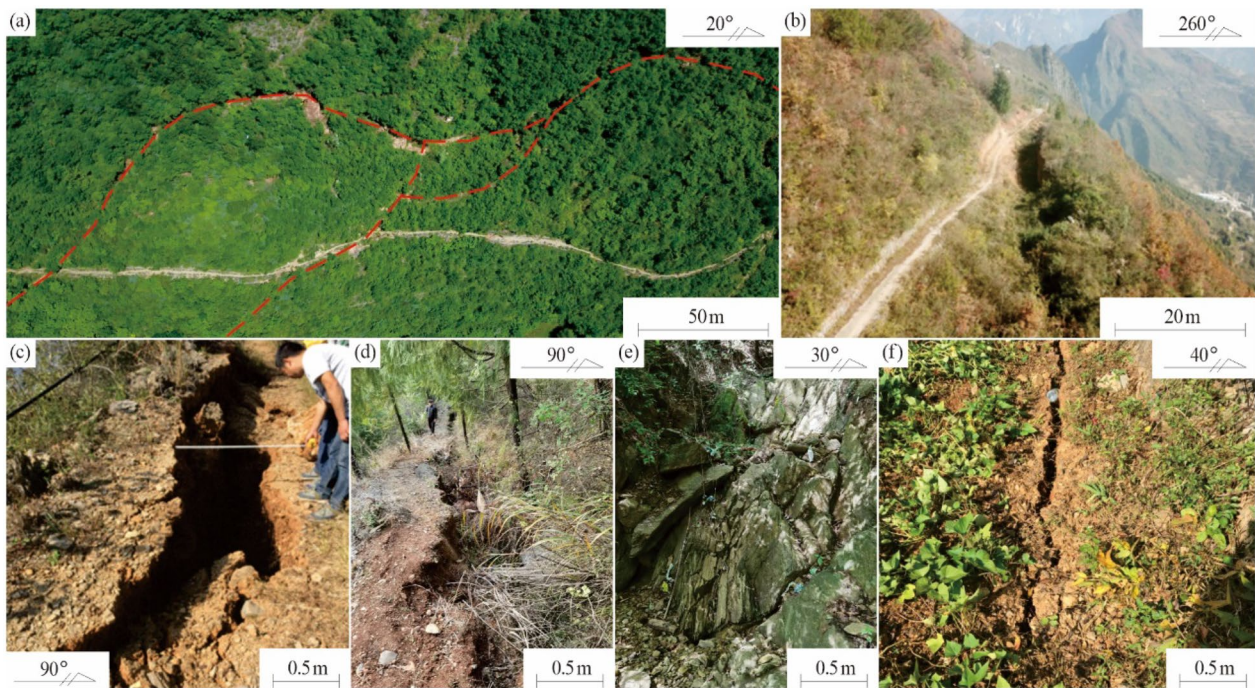


Fig. 7 Deformation features in PSA-III. **a** The main fracture belt at the rear edge, **b** a bulge with cracks near the Road-2, **c** a tension fissure in the middle and rear part, **d** a crack near the Road-2, **e** the seasonal gully on the eastern border and **f** a lateral fissure on the east side

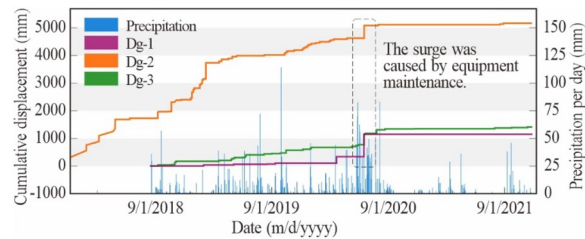


Fig. 8 Cumulative displacement of ground cracks in PSA-III

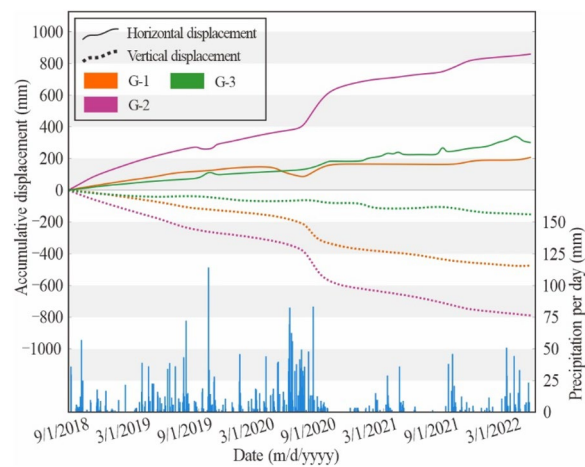


Fig. 9 Horizontal and vertical displacements in PSA-III measured by GNSS

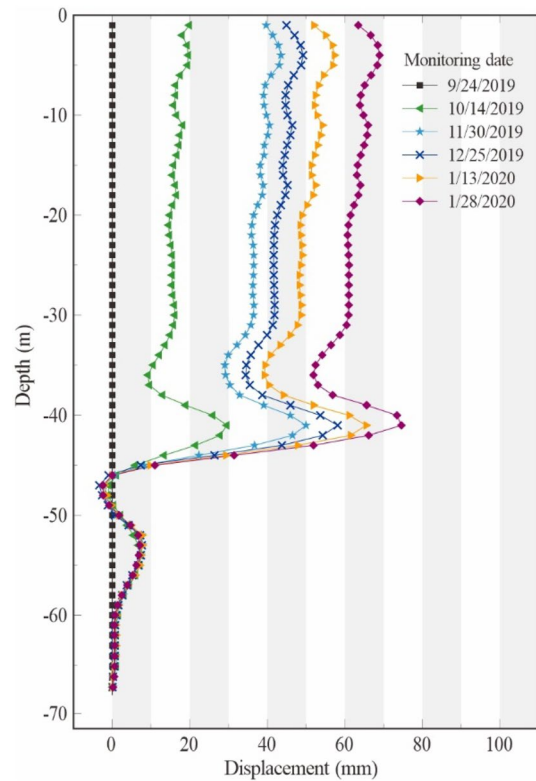


Fig. 10 Cumulative horizontal displacements measured by inclinometers

Instability model of continuous-pushing-section pressing locked-section

In this research, a new deformation mode was proposed from a novel perspective. This model can be referred to as the continuous-pushing-section pressing locked-section model which utilizes a progressive slope failure framework to explain the evolution pattern of large-scale anti-dip bedding rockslides. In this model, the typical deformation body is divided into two parts: the continuous pushing section and the locked section, as depicted in Fig. 11c. The evolving mode of continuous-pushing-section pressing locked-section was raised with 4 stages: initial stage, deformation increasing stage, pushing locked section stage and failure stage, as presented in Fig. 11.

- 1 Initial stage. At this stage, there is an obvious tensional fracture zone on the surface, which controls the trailing edge of the deforming body. There are tectonic fissures and joints within the rock mass as well, which are caused by the bending of strata, as shown in Fig. 11a. The overall deformation at this period is not distinct.
- 2 Deformation increasing stage. Affected by the internal and exterior long-term geological and environmental process including the dissolution process, the fragmentation of the rock near the main fracture zone on the ground deteriorates. The main fracture belt starts to extend along the brittle zone covered with fissures and joints generated by the bending deformation, as indicated in Fig. 11b. With the growth of the through zone, the rock formation

in the overlying pushing section would be cut and separated from the underlying rock bed completely. Under the effect of gravity, the pushing section creeps downward, pressing the adjacent rock layers along the potential sliding surface that have not been cut, and promoting the shear failure of the next layers. During this process, the displacement of the deforming slope shows a trend of steady increase. Then, as the creep process continues, the space available for creep inside the rock slope would decrease gradually. As a result, the deformation rate of the rock body would slow down in the later period, just as shown in Fig. 11e. In the meantime, there will be a slight bulge and small amounts of tension fissures locally on the ground surface under the pushing action.

- 3 Pushing locked section stage. When the through zone of the potential sliding surface extends to the front locked section, the continuous pushing section would load directly on the locked section by gravity. Concurrently, the overall deformation of the slope tends to be stable, as is shown in Fig. 11e, since there is little space available for compression inside the deformable body. On the other hand, the pushing effect on the locked rock mass would continue being strengthened, and obvious bulging mounds and tension fissures of certain scales would be formed on the surface.
- 4 Failure stage. When the locked section could not support the continuous pushing rock mass, it would fail in shear, resulting in the instability of the whole rock slope, as demonstrated in Fig. 11d.

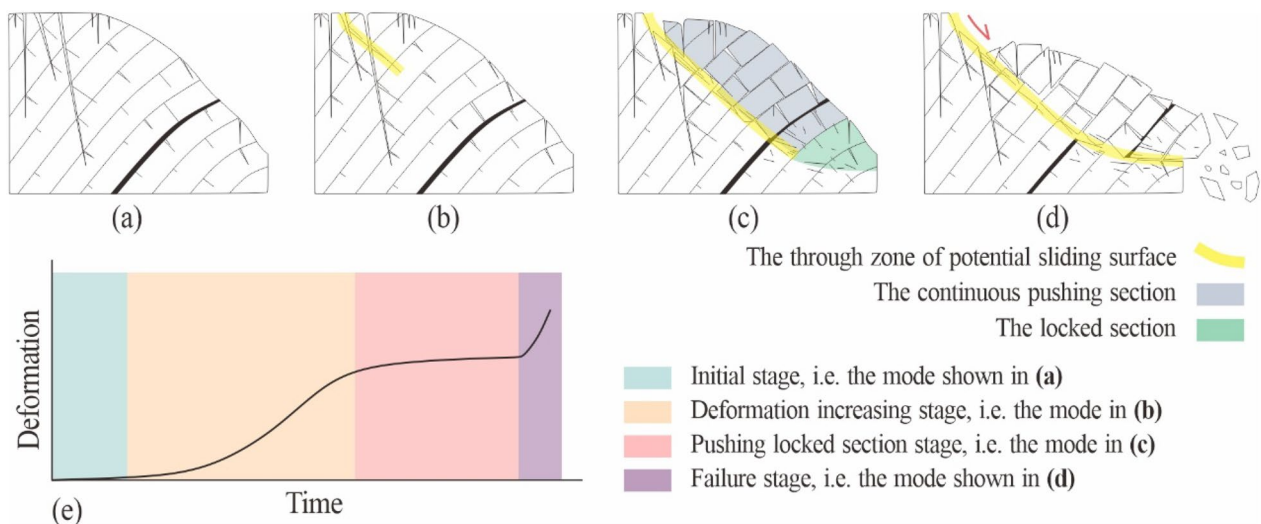


Fig. 11 The evolution mode of the large anti-dip bedding rockslide. **a** The initial stage, **b** the deformation increasing stage, **c** the pushing locked section stage, **d** the failure stage, and **e** the deformation trend of the continuous pushing section with time

It is noteworthy that the above four stages are not completely distinguished from each other. For example, a certain degree of landslide thrust could also be transferred to the locking section during the increasing deformation phase.

Deformation and instability mechanism of PSA-III

According to the proposed evolution mode of the large anti-dip bedding rockslide and the deformation characteristics supported by monitoring data, the deformation of PSA-III was estimated to be in the late period of the deformation increasing stage currently, with the movement deflecting to the slipped area, as shown in Fig. 6. The interpretation map of InSAR in Fig. 5 provides a visual representation of the binary structure of the locked section and the continuous pushing section. The rock mass near the crown of the slipped zone acts as the locked section, exhibiting surface bulges that indicate stress concentrations, as postulated by the evolution model. Field investigation also revealed the presence of bulging cracks, as depicted in Fig. 6 and Fig. 7b and d, further supporting the indications of stress concentrations in the rock mass near the crown of the slipped zone.

Correspondingly, the deforming of the continuous pushing section was increasing. As the rockslide body continues to deform, the continuous-pushing section gradually compresses and deforms, as exemplified in Fig. 11. Consequently, the cumulative displacement on the surface of the slope manifests as larger deformations as one moves further from the shear outlet. As the monitoring data show, Dg-2 specifically monitors the controlling rear crack of PSA-III, which inherently experiences the most substantial cumulative deformation. G-2 captures measurements from the middle region of the continuous-pushing-section, while G-3 is positioned close to the locked-section model. It is thus evident that Dg-2 records significantly greater cumulative deformation compared to G-2 and G-3. Meanwhile, the current slowing-down deformation trend that could be seen in Figs. 8 and 9 indicates that it is in the late period of the deformation-increasing stage, as described by the model proposed in this study.

In the future, with the sequential erosion of rainfall and the enhanced press from the pushing section, the rock bridges along the slipping plane would be damaged more seriously, the fractured rock mass would be compacted more densely and the voids would be eliminated over time. The deforming rate would keep on decreasing, and the cumulative subsequent deformation would level off gradually. However, the pushing on the locking section would sustain rising. As long as the pushing force exceeds the shear strength of the locked rock, the slope would be destroyed.

Besides, it is inferred that the shear capacity of the locked section of PSA-III might not be excellent because the locked rock is somewhat thin in width and there is no support on the other side of it but a steep cliff, which is exhibited in Figs. 2 and 3.

Discussion

Impact of precipitation on deformation

The deterioration of the Guang'an Village rockslide was affected by precipitation distinctly. On one hand, during the period from Sep. 1 to Oct. 21, 2017, the accumulated rainfall reached 575.60 mm, with a single-day maximum of 84.30 mm (Sep. 24, 2017), which promoted the rockslide event on Oct. 21, 2017, to some extent (Wang et al. 2019). On the other hand, the deformation of G-2 in Fig. 9 showed a significant uplift near Sep. 1, 2020, which seemed to be related to the previous intensive rainfall.

To determine the impact of rainfall on the Guang'an Village rockslide quantitatively, Pearson correlation coefficient (PCC) analysis was conducted based on the daily rainfall records and GNSS monitoring data in PSA-III (from Aug. 14, 2018, to May. 26, 2022). As one of the three major correlation coefficient methods, the PCC analysis is widely used in statistics (Wang et al. 2022).

For the preparation of the relationship analysis, the previous accumulated rainfall (PAR) and cumulative subsequent deformation (CSD) were organized into different data sets as feature vectors with various scales of time, as listed in Table 3. The time scale of 90 days was established through a process of trial. It is deemed appropriate when all the data within the designated time frame consistently demonstrate a gradual descent.

Table 3 Feature vectors of PAR and CSD within different time scales

Class	Vector	Description	
Feature vector of PAR	α_1	The rainfall of the day	
	α_2	PAR in the last 3 days	
	α_3	PAR in the last 6 days	
	\vdots	\vdots	
	α_{29}	PAR in the last 84 days	
	α_{30}	PAR in the last 87 days	
	α_{31}	PAR in the last 90 days	
	Feature vector of CSD	β_1	The deformation of the day
		β_2	CSD in the following 3 days
		β_3	CSD in the following 6 days
\vdots		\vdots	
β_{29}		CSD in the following 84 days	
β_{30}		CSD in the following 87 days	
β_{31}		CSD in the following 90 days	

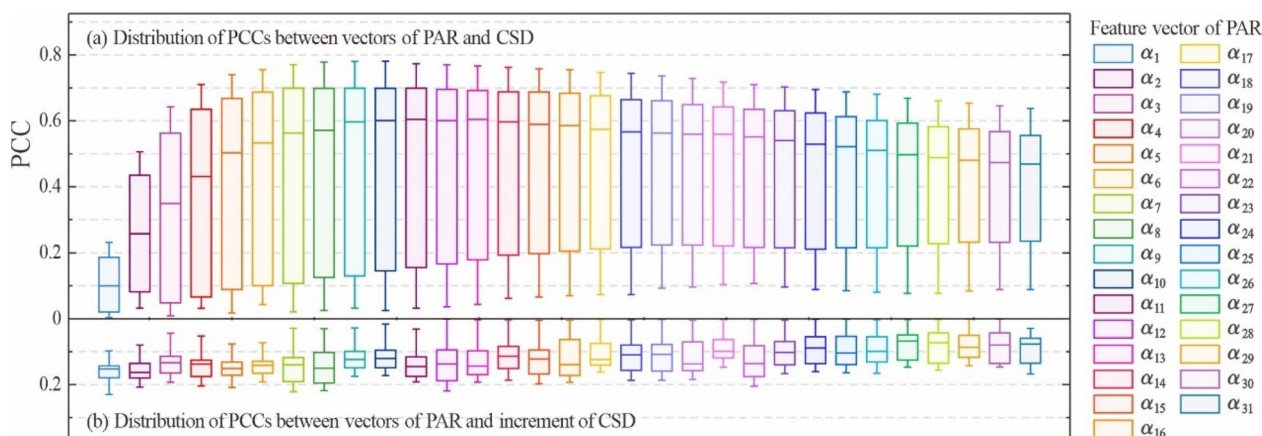


Fig. 12 Distributions of PCCs between vectors of PAR and both **a** CSD and **b** increment of CSD

After cross-calculating the PCCs between feature vectors of PAR and those of CSD from 3 GNSS points, respectively, they were consolidated into a single plot and reorganized as a series of boxplots associated with feature vectors of PAR, as shown in Fig. 12a. By the same method, the distribution of PCCs between PARs and the increments of CSD was obtained as well, which is presented in Fig. 12b. It reveals that the PCCs between PARs and CSDs are larger than those between PARs and the increments of CSD significantly. Within these data, the PCCs associated with G-2 show relatively higher values, whereas those associated with G-1 and G-3 exhibit comparatively lower values. However, there is an overall trend among all PCCs with respect to PARs, where they initially increase and then decrease with the expansion of the time scale.

Figure 13 demonstrates the cross-calculated PCCs between PARs and CSDs of 3 GNSS points, respectively. As to G-1 and G-2, the PCCs decrease after an initial rise with both PARs and CSDs with longer time duration. The PCC between α_{24} and β_{11} reaches the maximum value of 0.70 in G-1, while the top PCC of 0.78 appeared with α_{12} and β_9 as to G-2. For G-3, the PCCs present a smaller level compared to that of G-1 and G-2, although having a growth trend with the expanding of CSD around α_{11} .

To sum up, the precipitation has exerted a considerable influence on the deformation of PSA-III especially in the middle part. The impact would climb up at the first period, and then slacken off with the prolongation of time scale of both PAR and CSD. In G-2, the PCC arrived at 0.78 between CSD in the following 24 days and PAR in the last 33 days.

Evaluation of the instability mechanism

This study aims to analyze the deformation characteristics of the Guang’an Village rockslide based on existing

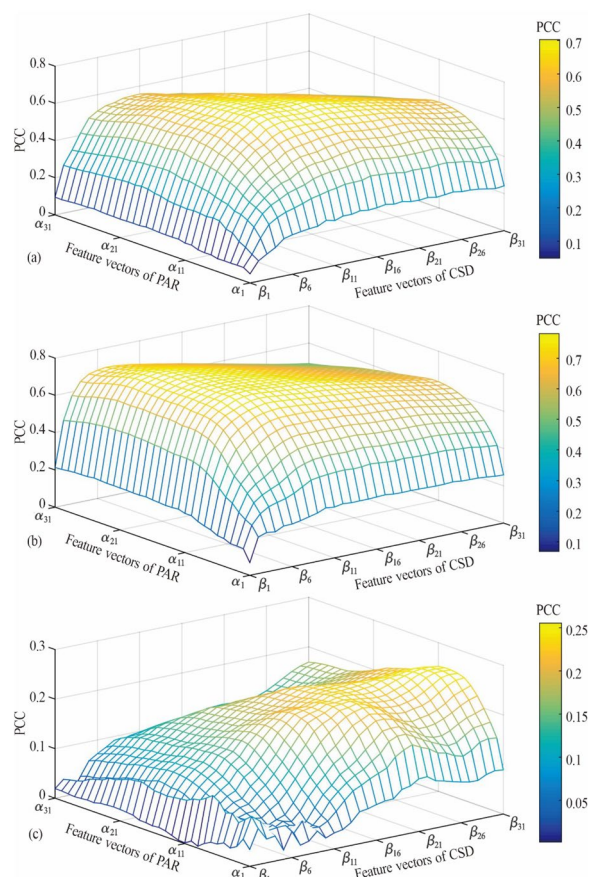


Fig. 13 Distributions of PCCs between vectors of PAR and CSD of **a** G-1, **b** G-2, and **c** G-3

data and propose a new evolutionary model to analyze the instability mechanism of PSA-III. The proposed model demonstrates good applicability for assessing the instability mechanism of PSA-III. However, the presence

of fragmented rock masses and complex deformation features resulting from the unique geological conditions of the Guang'an Village rockslide introduces a certain level of uncertainty in the deformation monitoring results of PSA-III. Consequently, this uncertainty may impact our interpretation of the instability mechanism of PSA-III to some extent.

Although there is substantial on-site evidence and monitoring data supporting the feasibility of using the proposed model to analyze the deformation and instability of PSA-III (as detailed in Sect. 5.3), it is important to note that certain data may be inconsistent with the findings of this study. For example, the Dg-1 curve in Fig. 8 does not exhibit a clear correlation with rainfall.

The study suggests that this kind of phenomenon could be attributed to that as the scale of the landslide is substantial, the observed displacements in monitoring data may reflect some localized characteristics rather than providing a holistic representation. Thus, in the analysis of landslide deformation trends based on in-situ monitoring data, it may be appropriate to selectively disregard such data when necessary.

The applicability of the instability model

The instability mechanism proposed in this paper is more applicable to large-scale natural rock slides with anti-dip bedding structures.

The application process of this model is as follows. After identifying a large-scale anti-dip bedding rockslide, the first step is to conduct a geological survey to determine the boundaries and spatial divisions of the landslide. The position of the sliding zone is then determined through drilling or geophysical methods. If there are noticeable tension cracks at the rear or if the sliding zone connects with tension cracks at the rear, it is an indication that this model may be applicable. In such cases, the front portion of the rockslide can be preliminarily classified as the locked section, while the middle and rear sections can be identified as the continuous-pushing section.

However, for some anti-dip rock slides that have been severely disturbed by human engineering or some small-scale landslides, the model proposed in this article is not applicable.

For some rocky landslides, especially those with cuts at the foot of the slope, the failure might not require the thought-out of the sliding surface. After the slope has been cut, the locked rock located at the foot of the slope would become so weak that might be destroyed by a minor disturbance before the development of the sliding plane (Sagaseta et al. 2001; Zhao et al. 2020). This situation is also common in indoor physical model tests, as the simple construction of the model can lead to the fragility of the rock in the locked section.

As to the small-scale anti-dip slopes, the deformation process is more likely to be the flexural toppling, block toppling, and the combination of the two, rather than obvious slippage. When the size of the rock slope is small, the geometry of the rock layers would be relatively large. This would result in the toppling or falling process of several pieces of rock dominoes, which has no significant sliding even when the headmost rock bar (the locked one) is crushed. This situation is common in physical experiments as well (Adhikary et al. 1997; Ding et al. 2021; Huang et al. 2022).

Monitoring of anti-dip slopes

Based on the instability mechanism of rock slopes with anti-dip bedding structure in this paper, it is recommended to observe the displacements of the slope in the continuous pushing section and monitor the in-situ stress of the rock in the locking section after the spatial distribution and potential sliding zone are determined. The deformation stage of the rock slide could be analyzed by the movement in the pushing section and the trend of the in-situ stress in the locking rock. Furthermore, the landslide warning could be achieved on the grounds of certain early warning models based on the evolution model of continuous-pushing-section pressing locked-section.

In addition, heavy rainfall in a single day or several days might not cause a large deformation of the entire rockslide immediately for the rock slope in the deformation-increasing stage. Therefore, the model designed for the early warning of large deformation of rockslides has to consider the long-term effect of continuous rainfall as well as the hysteresis of deformation.

Conclusion

Taking the Guang'an Village rockslide as an example, this paper studied the deformation characteristics of the anti-dip bedding rock landslide. Furthermore, the influencing factors and a novel instability mechanism were proposed. The specific conclusions are below:

- (1) The large-scale rockslide could be spatially divided into three parts: the slipped zone, the PSA, and the PTA. A catastrophic sliding event occurred in the slipped area on Oct. 21, 2017, following which the deformation of the PSA-III began to manifest and became evident gradually.
- (2) There are many factors affecting the deformation of the Guang'an Village rockslide. The source area has a sliding-prone geological structure of alternate hard and soft layers, with a reversely inclined rock bedding structure mainly dominated by tectonism and gravity. In addition, the rock bed is mainly

composed of limestone and shale, with coals locally, and mining activities have been carried out along the coal seams. Rainfall was the main trigger that promoted the deformation.

- (3) The failure mode of the anti-dip rock slope was considered to be continuous-pushing-section pressing locked-section. The PSA-III was in the late stage of the deformation-increasing phase according to the monitoring data. The rock mass in the continuous pushing section was still creeping along the fracture zone with the speed slowing down, while the surface of the locked section had begun to bulge.

Acknowledgements

The financial support is gratefully acknowledged. The authors also thank the editor and the anonymous reviewers for their insightful and constructive comments.

Author contributions

XW performed the data analysis and wrote the original draft. NZ provided the funding acquisition, and guided the revision of the paper. ZZ conducted the supervision and project administration. LW was a major contributor in visualization. SY was a major contributor in field investigation and data curation. PZ contributed to field investigation and data curation. GY contributed to the data analysis and validation. All authors read and approved the final manuscript.

Funding

This work was funded by the National Natural Science Foundation of China (U2244227); the Natural Science Foundation of Chongqing, China (CST-B2022NSCQ-MSX1650); and the Chongqing Planning and Natural Resources Bureau Research Project (KJ-2021047, KJ2023HT0015).

Availability of data and materials

The datasets used and/or analyzed during the current study are available from the corresponding author on reasonable request.

Declarations

Competing interests

The authors declare that they have no competing interests.

Received: 27 November 2023 Accepted: 3 March 2024

Published online: 29 March 2024

References

- Adhikary DP, Dyskin AV, Jewell RJ, Stewart DP (1997) A study of the mechanism of flexural toppling failure of rock slopes. *Rock Mech Rock Eng* 30(2):75–93. <https://doi.org/10.1007/BF01020126>
- Bucek R (1995) Toppling failure in rock slopes. PhD Thesis. University of Alberta, Edmonton, Canada
- Cruden DM (1989) Limits to common toppling. *Can Geotech J* 26(4):737–742. <https://doi.org/10.1139/t89-085>
- Cruden DM, Krahn J (1973) A reexamination of the geology of the frank slide. *Can Geotech J* 10(4):581–591. <https://doi.org/10.1139/t73-054>
- Cui FP, Li B, Xiong C, Yang ZP, Peng JQ, Li JS, Li HW (2022) Dynamic triggering mechanism of the Pusa mining-induced landslide in Nayong County, Guizhou Province. *China Geomat Nat Haz Risk* 13(1):123–147. <https://doi.org/10.1080/19475705.2021.2017020>
- Dai ZW, Zhang CY, Wang L, Fu YP, Zhang Y (2021) Interpreting the influence of rainfall and reservoir water level on a large-scale expansive soil landslide in the Danjiangkou Reservoir region. *China Eng Geol* 288:106110. <https://doi.org/10.1016/j.enggeo.2021.106110>
- de Freitas MH, Watters RJ (1973) Some field examples of toppling failure. *Géotechnique* 23(4):495–513. <https://doi.org/10.1680/geot.1973.23.4.495>
- Ding BD, Han ZY, Zhang GC, Beng XT, Yang YC (2021) Flexural toppling mechanism and stability analysis of an anti-dip rock slope. *Rock Mech Rock Eng* 54(8):3721–3735. <https://doi.org/10.1007/s00603-021-02435-w>
- Gao SH, Meng HJ, Wu YF, Wang XB, Wang Y, Wu JH, Wang P (2023) Examination of the effects of different frequencies on rock fracturing via laboratory-scale variable amplitude fatigue loading experiments. *Appl Sci-Basel* 13(8):4908. <https://doi.org/10.3390/app13084908>
- Goodman RE, Bray JW (1976) Toppling of rock slopes. Proceedings of ASCE specialty conference on rock engineering for foundations and slopes, Colorado, Boulder. 201–234.
- Gu DM, Huang D (2016) A complex rock topple-rock slide failure of an anacinal rock slope in the Wu Gorge, Yangtze River. *China Eng Geol* 208:165–180. <https://doi.org/10.1016/j.enggeo.2016.04.037>
- Huang RQ, Li WL (2011) Formation, distribution and risk control of landslides in China. *J Rock Mech Geotech* 3(2):97–116. <https://doi.org/10.3724/SPJ.1235.2011.00097>
- Huang BL, Yin YP, Liu GN, Wang SC, Chen XT, Huo ZT (2012) Analysis of waves generated by Gongjiafang landslide in Wu Gorge, three Gorges reservoir, on November 23, 2008. *Landslides* 9(3):395–405. <https://doi.org/10.1007/s10346-012-0331-y>
- Huang D, Ma H, Huang RQ, Peng JB, Luo SL (2022) Deep-seated toppling deformations at the dam site of the Miaowei Hydropower Station. *Southwest China Eng Geol* 303:106654. <https://doi.org/10.1016/j.enggeo.2023.107228>
- Li ZW, Liu SG, Luo YH, Liu S, Xu GQ (2007) Structural style and deformation mechanism of the southern Dabashan foreland fold-and-thrust belt, central China. *Front Earth Sci China* 1:181–193. <https://doi.org/10.1007/s11707-007-0023-4>
- Liu M, Liu FZ, Huang RQ, Pei XJ (2016) Deep-seated large-scale toppling failure in metamorphic rocks, a case study of the Erguxi slope in southwest China. *J Mt Sci-Engl* 13(12):2094–2110. <https://doi.org/10.1007/s11629-015-3803-4>
- Ng CWW, Guo HW, Ni JJ, Zhang Q, Chen ZK (2022) Effects of soil-plant-biochar interactions on water retention and slope stability under various rainfall patterns. *Landslides* 19:1379–1390. <https://doi.org/10.1007/s10346-022-01874-y>
- Qi SW, Wu FQ, Yan FZ, Lan HX (2004) Mechanism of deep cracks in the left bank slope of Jinping first stage hydropower station. *Eng Geol* 73(1):129–144. <https://doi.org/10.1016/j.enggeo.2003.12.005>
- Qin PP, Huang BL, Li B, Chen XT, Jiang XN (2022) Hazard analysis of landslide blocking a river in Guang'an Village, Wuxi County, Chongqing. *China Landslides* 19(11):2775–2790. <https://doi.org/10.1007/s10346-022-01943-2>
- Reid G, Stewart D (1986) A large scale toppling at Afton. Proceedings of International Symposium on Geotechnical Stability in Surface Mining. Calgary, Rotterdam. 215–223
- Sagaseta C, Sánchez JM, Cañizal J (2001) A general analytical solution for the required anchor force in rock slopes with toppling failure. *Int J Rock Mech Min* 38(3):421–435. [https://doi.org/10.1016/S1365-1609\(01\)00011-9](https://doi.org/10.1016/S1365-1609(01)00011-9)
- Wang LQ, Yin YP, Huang BL, Zhang ZH, Wei YJ (2019) Formation and characteristics of Guang'an Village landslide in Wuxi, Chongqing. *China Landslides* 16(1):127–138. <https://doi.org/10.1007/s10346-018-1086-x>
- Wang XB, Wang LQ, Zhang WG, Zhang CS, Tan CX, Yan P, Zhang ZH, Guo J (2022) Ground fissure susceptibility mapping based on factor optimization and support vector machines. *B Eng Geol Environ* 81(8):341. <https://doi.org/10.1007/s10064-022-02843-4>
- Wang L, Wu CZ, Yang ZY, Wang LQ (2023) Deep learning methods for time-dependent reliability analysis of reservoir slopes in spatially variable soils. *Comput Geotech* 159:105413. <https://doi.org/10.1016/j.compgeo.2023.105413>
- Yin YP, Huang BL, Wang WP, Wei YJ, Ma XH, Ma F, Zhao CJ (2016) Reservoir-induced landslides and risk control in Three Gorges Project on Yangtze River. *China J Rock Mech Geotech* 8(5):577–595. <https://doi.org/10.1016/j.jrmge.2016.08.001>

- Yin YP, Li B, Gao Y, Wang WP, Zhang SL, Zhang N (2023) Geostructures, dynamics and risk mitigation of high-altitude and long-runout rockslides. *J Rock Mech Geotech* 15:66–101. <https://doi.org/10.1016/j.jrmge.2022.11.001>
- Yin BG, Yin YP, Zhang M, Zhang CY, He Q, Wang GH (2024) Active fault control led to the Moli landslide triggered by rainfall on 26 February 2021 in Zhouqu County, Gansu, China. *Landslides* 21:83–98. <https://doi.org/10.1007/s10346-023-02175-8>
- Zhang CY, Yin YP, Yan H, Li HX, Dai ZW, Zhang N (2021) Reactivation characteristics and hydrological inducing factors of a massive ancient landslide in the three Gorges Reservoir. *China Eng Geol* 292:106273. <https://doi.org/10.1016/j.enggeo.2021.106273>
- Zhang CY, Dai ZW, Tan WJ, Yang YT, Zhang LH (2022a) Multiscale study of the deterioration of sandstone in the Three Gorges Reservoir area subjected to cyclic wetting-cooling and drying-heating. *Rock Mech Rock Eng* 55:5619–5637. <https://doi.org/10.1007/s00603-022-02929-1>
- Zhang CY, Yin YP, Yan H, Zhu SN, Li B, Hou XF, Yang YT (2022b) Centrifuge modelling of multi-row stabilizing piles reinforced reservoir landslide with different row spacings. *Landslides* 20(3):559–577. <https://doi.org/10.1007/s10346-022-01994-5>
- Zhang K, Gong FM, Li L, Ng AH-M, Liu PF (2022c) Mapping the long-term evolution of the post-event deformation of the Guang'an Village landslide, Chongqing, China Using Multibaseline InSAR Techniques *Forests* 13:887. <https://doi.org/10.3390/f13060887>
- Zhang YF, Tie YB, Wang LQ, Liu JF (2022d) CT scanning of structural characteristics of glacial till in Moxi River Basin, Sichuan Province. *Appl Sci-Basel* 12:3040. <https://doi.org/10.3390/app12063040>
- Zhang CY, Yin YP, Yan H, Zhu SN, Zhang M, Wang LQ (2023a) Centrifuge modelling of unreinforced and multi-row stabilizing piles reinforced landslides subjected to reservoir water level fluctuation. *J Rock Mech Geotech*. <https://doi.org/10.1016/j.jrmge.2023.09.025>
- Zhang YF, Zhang WG, Wang LQ, Xiao T, Meng XY, Zhang ZH (2023b) Mechanism of the high-speed and long-run-out landslide considering the evolution of the frictional heat in the sliding zone. *Nat Hazards*. <https://doi.org/10.1007/s11069-023-06334-x>
- Zhang WG, Lin SC, Wang LQ, Wang L, Jiang X, Wang S (2024) A novel creep contact model for rock and its implement in discrete element simulation. *Comput Geotech* 167: <https://doi.org/10.1016/j.compgeo.2023.106054>
- Zhao W, Wang RQ, Nian TK (2020) Stability analysis of anti-dip rock slopes with flexural toppling failure based on deformation compatibility. *Rock Mech Rock Eng* 53:3207–3221. <https://doi.org/10.1007/s00603-020-02098-z>
- Zhou C, Hu YJ, Xiao T, Ou Q, Wang LQ (2023) Analytical model for reinforcement effect and load transfer of pre-stressed anchor cable with bore deviation. *Constr Build Mater* 379:131219. <https://doi.org/10.1016/j.conbuildmat.2023.131219>

Publisher's Note

Springer Nature remains neutral with regard to jurisdictional claims in published maps and institutional affiliations.